Chapter 10
Creation of Blue Light Emitting Color Centers in Nanosized Diamond for Different Applications

L. Himics, S. Tóth, M. Veres, A. Czitrovszky, A. Nagy, D. Oszetzky, A. Kerekes, Sz. Kugler, I. Rigó, A. Tóth, and M. Koós

Abstract Plasma immersion ion implantation and focused ion beam treatment techniques were used to create nitrogen-related complex defect centers in detonation nanodiamond crystals. Helium implantation was used to produce vacancies in the crystal structure, which was followed by the introduction of nitrogen ions (with the same method). Heat treatment at 1,023 K was applied to initiate vacancy diffusion and formation of complex defect centers. The sp^2 carbon content of the samples formed during the implantation and the high-temperature annealing was decreased by oxidation at 723 K in air. Changes in the bonding structure were monitored by Raman and infrared spectroscopic measurements after each step of the defect creation process. It was found that the photoluminescence of nanosized diamond changes remarkably as a consequence of different treatments and a new, narrow, intense emission band develops in the deep blue wavelength region. The N3 nitrogen-related complex defect center was considered as source of this fine structured emission band in the luminescence spectrum.

Keywords Nanodiamond • Nitrogen-related complex color centers • Ion implantation • Photoluminescence

L. Himics • S. Tóth • M. Veres (✉) • A. Czitrovszky • A. Nagy • D. Oszetzky • A. Kerekes
Sz. Kugler • I. Rigó • M. Koós
Wigner Research Centre for Physics, Hungarian Academy of Sciences, P.O.B. 49,
H-1525 Budapest, Hungary
e-mail: veres.miklos@wigner.mta.hu

A. Tóth
Institute of Materials and Environmental Chemistry, Research Centre for Natural Sciences,
Hungarian Academy of Sciences, H-1525 Budapest, Hungary

P. Petkov et al. (eds.), *Nanoscience Advances in CBRN Agents Detection, Information and Energy Security*, NATO Science for Peace and Security Series A: Chemistry and Biology, DOI 10.1007/978-94-017-9697-2_10

10.1 Introduction

Due to its unique properties, which provide a good basis for many important applications and technologies now and in future, nanodiamond (ND) gained much scientific attention from many research groups in the last decades. Particular interest is devoted to the light emitting properties of different color centers in diamond [1–3]. Most of these emit in the green-red wavelength region, but some, like the so-called "N3" optically active defect, detected first in natural diamond, emit in the UV or near-UV range. The N3 center has excellent emission properties, which make it a good candidate as a active laser material for color center lasers, for example. It was shown that the N3 center is thermally stable up to temperatures above 800 K and exhibits no photobleaching even at extremely high power densities (up to 100 MW/cm^2) [4]. It consists of three substitutional nitrogen atoms situated in the (111) plane around a carbon vacancy in the diamond crystal and has $C_{3\nu}$ point symmetry [5]. In the case of the optically active N3 defect the zero phonon line (ZPL) (characteristic parameter of different color centers allowing also the identification of luminescent point defects in diamond) appears at 2.985 eV (415 nm) in the photoluminescence (PL) spectrum. This center was observed earlier in artificial single crystal CVD diamond films and also after intentional nitrogen ion implantation of IIa type diamonds [4]. The situation for nanosized diamond, more actual for nanotechnological applications, is not so auspicious. Except some literature data on the detection of optically active N3 defect centers [6] theirintentional creation in ND was not demonstrated earlier.

In this paper we report on the formation of N3 color center ins detonation nanodiamond crystals with average grain size below 20 nm using ion implantation and subsequent heat treatments.

10.2 Experimental Details

10.2.1 Preparation of the ND Samples

"Layers" were prepared from nanodiamond powders in order to eliminate handling difficulties of the samples during the different treatments and investigations. Commercially available detonation ND powder (Neomond Ltd.) was mixed with distilled water and subjected to ultrasonication for 3 h. The concentration of ND in the suspension was 1.5 mg/ml. After sonication 1,500 ml of ND slurry was dripped into a 10 mm hole of a stainless steel ring placed on a silicon substrate. The ring was used to limit the surface covered by the ND suspension. The samples were dried in air for at least 48 h at room temperature. After removal of the ring a circular stain of ND "film" was left on the silicon surface.

10.2.2 Treatments

Samples were implanted using two different implantation methods: Plasma Immersion Ion Implantation (PIII) and Focused Ion Beam (FIB) treatment with different energies and fluences.

An acceleration voltage of $U = 20$ kV and a fluence of $F = 10^{15}$ ion/cm^2 were used during the PIII treatment. The samples were implanted first with He^+ ions, followed by the N^+_2 treatment.

For the FIB technique the acceleration voltage was $U = 2$ kV, and fluences of $F = 1.8 \times 10^{15}$ ion/cm^2 and $F = 1.5 \times 10^{15}$ ion/cm^2 were used during He^+ and N^+_2 ion bombardment, respectively. The implanted samples were heat treated at 1,023 K for 2 h in vacuum, then annealed at 723 K for 5 h in air.

10.2.3 Characterization Techniques

Raman spectra of the samples were recorded in the 1,000–2,000 cm^{-1} region with a Renishaw 1,000 Raman spectrometer equipped with a Leica microscope. The 488 nm line of an argon ion laser served as excitation source. After baseline correction all spectra were normalized to the maximal intensity in the D-band region and shifted along the ordinate for better visibility.

Fourier-transform infrared spectroscopic measurements were performed in the 1,000–2,000 cm^{-1} wavenumber region using a Bruker IFS28 FTIR spectrometer attached to a microscope. The samples were tilted in order to eliminate interference effects in the spectra.

Steady state photoluminescence was measured at room temperature in front face geometry using a Horiba Jobin Yvon Fluorolog FL3-22 fluorimeter with a 450 W xenon lamp as an excitation source. The spectral luminescence distribution of was analyzed in the 1.8–4.25 eV photon energy range using 4.597 eV excitation. The measured spectra were corrected for the spectral response of the system and for the excitation intensity. The spectral resolution was between 4 and 17 meV.

10.2.4 SRIM Calculations

The Stopping and Range of Ions in Matter (SRIM) [7] computer program, a widely used Monte-Carlo-simulation based software for the prediction of the stopping depth of different ions in different structures of solid materials, was used to estimate the depth distributions of the implanted ions and generated vacancies for 20 keV / (PIII) and 2 keV (FIB) ions. Modelling parameters were: 3.15 g/cm^3 for the density of nanodiamond, 45 eV for the displacement energy and 4.3 eV for the surface binding energy [8–10] in both cases.

10.3 Results and Discussion

10.3.1 SRIM Calculations

Figure 10.1 shows the result of SRIM calculations. Since the fluences used with PIII and FIB were similar, the acceleration voltage is the main parameter being different for the two treatments. It can be seen that helium ion implantation with 20 keV energy creates vacancies in the 2–160 nm range with a maximum around 80 nm, while a ten times lower ion energy results in a five times shallower vacancy distribution (2–30 nm). The results for the nitrogen ion distributions are similar. While for 20 keV the nitrogen ion distribution is in the range of 1–60 nm, the lower ion energy resulted in a five times shallower implantation region (1–11 nm). The formation of nitrogen-vacancy complexes is expected to be of highest probability in the depth region where the vacancy and nitrogen distributions overlap. However, the maximum of the distribution of complexes is slightly shifted to lower depths, since vacancies are also generated by the nitrogen implantation (black curve on Fig. 10.1) which can take part in the formation of complex centers too.

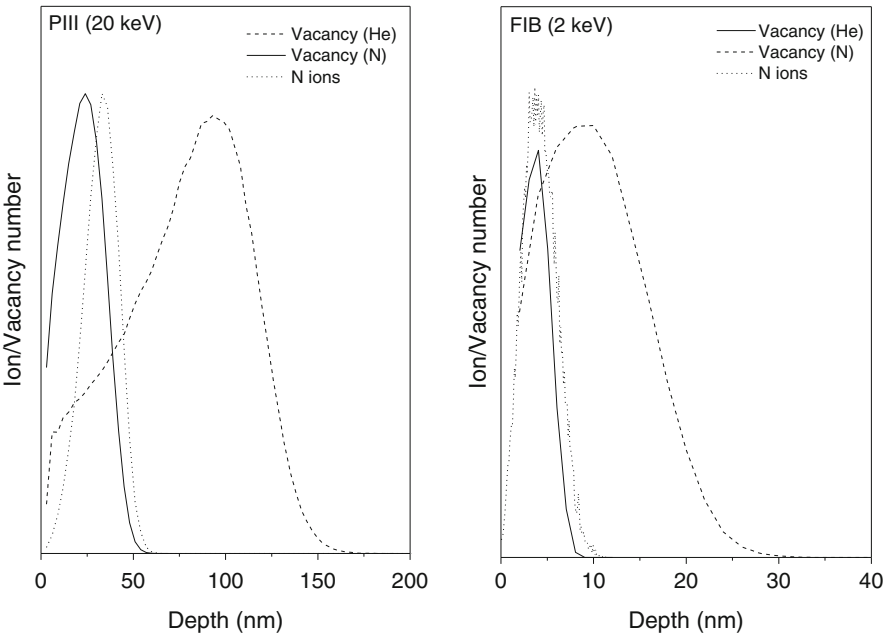

Fig. 10.1 The calculated depth distribution of vacancies generated by helium and nitrogen ions, and of nitrogen-vacancy complex centers during 20 keV PIII and 2 keV FIB treatments

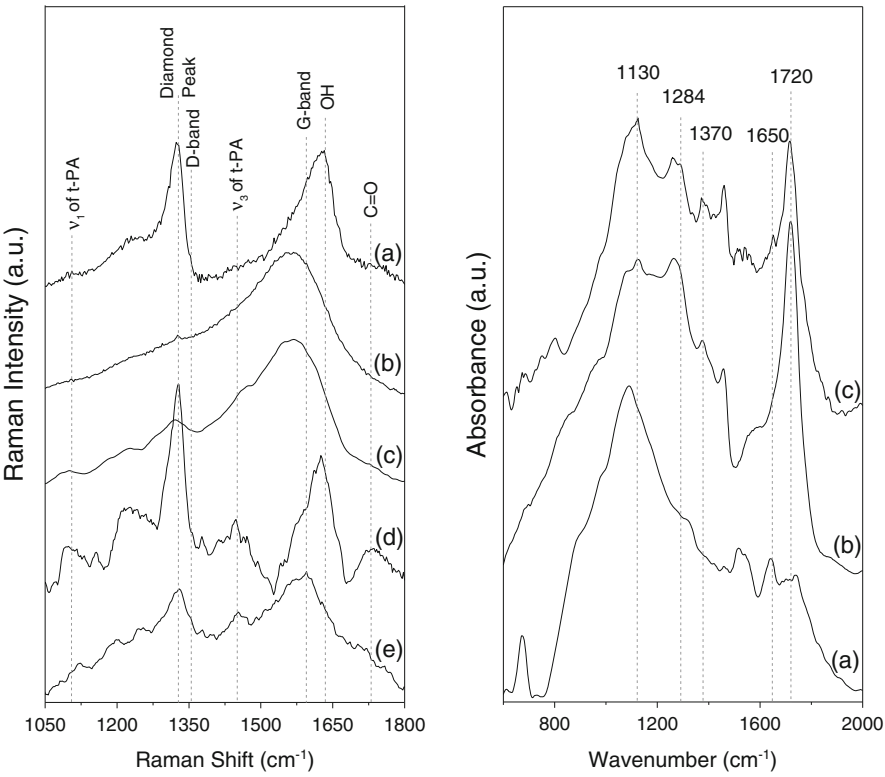

Fig. 10.2 *Left*: Raman spectra of nanodiamond samples measured after different treatments: (**a**) untreated, after He^+ and N_2^+ ion implantation by (**b**) PIII and (**c**) FIB techniques and after complex heat treatment of the (**d**) 20 keV and (**e**) 2 keV samples. *Right*: FTIR spectra of nanodiamond samples measured after different treatments: (**a**) untreated, after He^+ and N_2^+ ion implantation and complex heat treatment by the (**b**) PIII and (**c**) FIB techniques

10.3.2 Raman and FTIR Investigations

The Raman spectrum of an untreated sample is typical for small crystallite size ND ((a) in the left panel of Fig. 10.2). Due to the confinement effect the characteristic diamond peak is shifted to lower wavenumbers and it is located at 1,324 cm^{-1}. Following the algorithm described in Ref. [11] and fitting the peak, the average grain size was estimated to be around 12 nm for our sample. D and G bands characteristic for amorphous carbon material can be seen around 1,355 and 1,590 cm^{-1} respectively. Other types of impurities assigned to surface functional groups like OH (peak at 1,640 cm^{-1}) and oxygen (peak at 1,740 cm^{-1}) were also detected in the spectrum of the sample. The weak so called "nanodiamond finger-print" peaks (attributed to the υ_1 and υ_3 modes of trans-polyacetylene (t-PA)) can be seen at 1,120 and 1,455 cm^{-1}, respectively [12].

Both ion implantation techniques affect the character of the Raman spectra remarkably ((b) and (c) in the left panel of Fig. 10.2). The spectrum of the PIII sample is now dominated by the G band of graphitic carbon.

Due to the increased, broad background in the D band region the diamond peak is very weak, but still detectable. This finding indicates that the PIII treatment causes graphitization of the diamond structure and the surface of the diamond crystallites is transformed into graphitic amorphous carbon. The FIB implantation has less impact on the bonding structure of the diamond sample, mainly because of the ion energy one order of magnitude lower. The Raman spectrum of the FIB implanted sample also contains the characteristic D and G bands, but compared to the PIII case they contribute less to the scattering.

As a result of the complex heat treatments, performed at 1,023 K in vacuum and at 723 K in air, the bonding structure of both types of samples has changed remarkably ((d) and (e) on the left panel of Fig. 10.2). It is known that high temperature annealing initiates vacancy migration and induces relaxation of the implanted structure, while the oxidation in air at lower temperatures removes the sp^2 hybridized carbon content. After the treatments the diamond peak has become more pronounced, especially in the PIII treated sample. The oxidation reduced the non-diamond content in both samples, as is indicated by the remarkable decrease of G band intensity. The "fingerprint" peaks can also be seen again in the spectra recorded after the heat treatments.

FTIR spectroscopy was used to prove the presence of nitrogen impurities in the nanodiamond structure [13]. New features were observed in the spectra recorded after different treatments (right panel in Fig. 10.2), compared to the untreated sample. The appearance of characteristic bands at 1,130, 1,284 and 1,370 cm^{-1} after both PIII and FIB implantation evidences the introduction of nitrogen into the nanodiamond structure. Peaks at 1,130 and 1,284 cm^{-1}, appearing as weak shoulders of a broad band, can be attributed to substitutional nitrogen and the more complex N2 center consisting of two neighboring nitrogen atoms, respectively. The third peak at 1,370 cm^{-1} is observable as an individual band, but has a lower intensity than the former two. This band can be assigned to the N3 center, containing three or more adjacent nitrogen atoms. Detection of the above described nitrogen complexes in the implanted diamond structures is in good agreement with the SRIM calculations predicting a relatively narrow depth distribution of the nitrogen ions, which means a relatively high nitrogen concentration in the implanted regions.

10.3.3 Photoluminescence

From the results of the SRIM calculations and the significant differences between the Raman and FTIR spectra of untreated and ion implanted ND samples remarkable changes can be expected also in the electronic structure of the investigated nanodiamond samples. Its can be studied optically by photoluminescence spectroscopy, which is widely used for the characterization of impurities and defects in

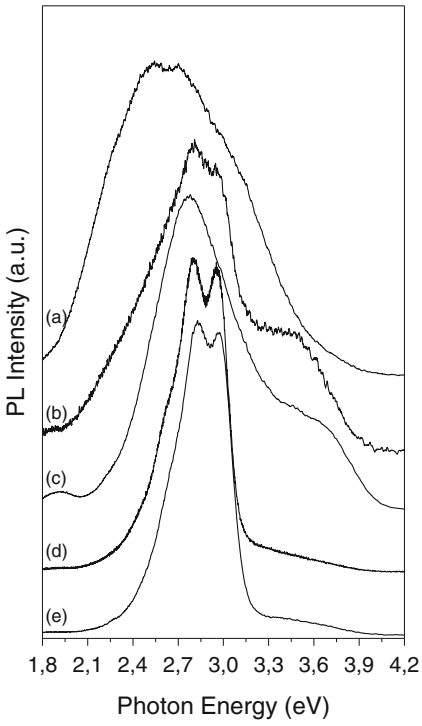

Fig. 10.3 Photoluminescence spectra of (**a**) untreated, (**b**) PIII and (**c**) FIB implanted samples. Curves (**d**) and (**e**) are PL spectra taken after complex heat treatment of PIII and FIB treated samples, respectively. All spectra were normalized to the maximal peak intensity and shifted along ordinate for clarity

diamond structures [14]. Due to the well-defined structure of optically active point defects, the strong carbon-carbon bond and the relatively weak electron-phonon interaction, PL allows easy identification of color centers in the diamond structure [15].

Figure 10.3 shows the evolution of the PL spectra after different treatments. The PL spectrum of the untreated material excited with by $E_{ex} = 4.597$ eV photons (Fig. 10.3a) has a wide broad feature typical for small size nanocrystalline diamond and was observed by many research groups [16, 17]. This broad band is explained as a result of overlapping of narrow peaks attributed mainly to different functional groups on crystallite surfaces and to structural defects created during the detonation process [17].

Curves (b) and (c) in Fig. 10.3 show the effect of He^+ and N_2^+ ion implantations on the PL spectra for the PIII and FIB cases. PIII implantation causes considerable modification of the PL band; at least three spectral components became distinguishable near 2.85, 3.09 and 3.6 eV photon energies. A small enhancement on the low energy side near 2.3 eV can also be observed. In addition, the emission intensity is decreased remarkably, as it can be seen from the signal-to-noise ratio. The unresolved components around 3.6 eV are related to different types and combinations of nitrogen defects and vacancies [4] and indicate the formation of nitrogen-related defects during the implantation. The emission band in the 2.7–3.0 eV range can be assigned to the well known N3 color center. The enhancement around 2.3 eV is due to non-diamond carbon structures created by the implantation.

The FIB treatment causes similar changes in the PL spectrum as PIII (Fig. 10.3c), but the dramatic decrease of the signal-to-noise ratio was not observed. Since the lower ion energy used in FIB implantation is less destructive, less sp^3 hybridized carbon atoms transform into emission-quenching sp^2 ones compared to PIII. This is also supported by the Raman measurements (Fig. 10.2). A well pronounced broad luminescence band with a maximum around 2.75 eV appears in the spectrum of the FIB implanted sample overlaps with a broad band at higher energies. This band can be related to substitutional nitrogen and other nitrogen-related defects in the structure [18].

PL spectra recorded with the implanted samples show that both implantation techniques are suitable for the introduction of nitrogen into the ND structure, but the formation of "good quality" complex centers requires further treatments. Curves (d) and (e) in Fig. 10.3 represent the PL spectra after heat treatments of the PIII and FIB samples. Well defined emission bands developed in both cases, the detailed analysis of which proves the formation of N3 defect centers: the zero phonon line at 2.98 eV and the phonon side bands at lower photon energies, partially resolved at 2.83 and 2.71 eV, are characteristic for this type of defect in diamond. The phonon replica with 150 and 120 meV spacings are slightly different from those observed for large diamond crystals, but this is due to the differences in local phonon modes of nanocrystalline and macroscopic diamond.

10.4 Conclusions

A relatively intense deep blue light emission band, attributed to the N3 complex defect center was obtained in nanosized diamond with average grain sizes below 20 nm by He^+ and N_2^+ implantation using 20 keV and 2 keV ion energies and subsequent heat treatments. Raman and infrared spectroscopies show remarkable changes in the bonding configuration of the samples after the different treatments and proved the introduction of nitrogen and the formation of complex nitrogen-related defect centers in the diamond structure, the light emission properties of which were examined by PL measurements. Our results demonstrate the effectiveness of low-energy implantation methods for the formation of light emitting centers in nanodiamonds.

References

1. Aharonovich I, Castelletto S, Simpson DA, Su C-H, Greentree AD, Prawer S (2011) Rep Prog Phys 74:076501. doi:10.1088/0034-4885/74/7/076501
2. Fu C-C, Lee H-Y, Chen K, Lim T-S, Wu H-Y, Lin P-K, Wei P-K, Tsao P-H, Chang H-C, Fann W (2007) Natl Acad Sci 104:727
3. Aharonovich I, Greentree AD, Prawer S (2011) Nat Photonics 5:397
4. Zaitsev AM (2001) Optical properties of diamond. Springer, Berlin/New York

5. Stephen C, Rand L, DeShazer G (1987) US Patent US4638484 A, 20 Jan 1987
6. Mikov SN, Igo AV, Gorelik VS (1999) Phys Solid State 41:1012
7. Ziegler JF, Ziegler MD, Biersack JP (2010) Nucl Inst Methods B 268:1818
8. Vereshchagin AL, Sakovich GV (2001) Mendeleev Commun 11:39
9. Koike J, Parkin DM, Mitchell TE (1992) Appl Phys Lett 60:1450
10. Ullmann J, Delan A, Schmidt G (1993) Diam Relat Mater 2:266
11. Osswald S, Mochalin VN, Havel M, Yushin G, Gogotsi Y (2009) Phys Rev B 80:075419
12. Ferrari AC, Robertson J (2001) Phys Rev B 63:121405
13. Hsiao-Chi L, Bing-Ming C (2011) Anal Chem 83:6539–6544
14. Zaitsev AM, Melnikov AA, Denisenko AV, Varichenko VS, Job R, Fahrner WR (1996) Mater Res Soc Symp Proc 416:113
15. Collins AT (1992) Diam Relat Mater 1:457
16. Mochalin VN, Shenderova O, Ho D, Gogotsi Y (2012) Nat Nanotechnol 7:11
17. Schrand AM, Ciftan Hens SA, Shenderova OA (2009) Crit Rev Solid State Mater Sci 34:18
18. Eaton-Magana S, Post JE, Heaney PJ, Walters RA, Breeding CM, Butler JE (2007) Gems Gemol 43:332